Vol. 508: 33–51, 2014
doi: 10.3354/meps10871

MARINE ECOLOGY PROGRESS SERIES
Mar Ecol Prog Ser

Published August 4

Geospatial statistics strengthen the ability of natural geochemical tags to estimate range-wide population connectivity in marine species

Sara E. Simmonds[1,*], Brian P. Kinlan[2,3], Crow White[4], Georges L. Paradis[5], Robert R. Warner[6], Danielle C. Zacherl[7]

[1]Department of Ecology and Evolutionary Biology, University of California, Los Angeles, CA 90095-1606, USA
[2]Biogeography Branch, Center for Coastal Monitoring and Assessment, National Centers for Coastal Ocean Science, NOAA National Ocean Service, Silver Spring, MD 20910-3281, USA
[3]Consolidated Safety Services, Inc., Fairfax, VA 22030, USA
[4]Biological Sciences Department, California Polytechnic State University, San Luis Obispo, CA 93407, USA
[5]Marine Science Institute, University of California, Santa Barbara, CA 93106, USA
[6]Department of Ecology, Evolution and Marine Biology, University of California, Santa Barbara, CA 93106, USA
[7]Department of Biological Science, California State University Fullerton, CA 92834-6850, USA

ABSTRACT: Using calcified structures as natural geochemical tags to estimate levels of population connectivity is becoming increasingly common. However, the technique suffers from several logistical and statistical problems that constrain its full application. Foremost is that only a subset of potential sources is sampled, often compounded by under-sampling within locations at an overly coarse spatial scale. This introduces unknown error and prevents the creation of a range-wide connectivity matrix. To address this issue, we analyzed the natural geochemical tags of embryonic statoliths in the whelk *Kelletia kelletii* (Forbes, 1850). We sampled from 23 sites over the entire geographic range in 2004 and 2005 from Monterey (California, USA) (36°N) to Isla Asunción, (Baja California, Mexico) (27°N). We then used geospatial statistics (kriging) to make continuous along-coast maps of embryonic statolith chemistry. This allowed us to estimate chemistry at unsampled locations. We used this new continuous assignment method to estimate the spatial error associated with assignment by the classic method of discriminant function analysis (DFA). Then, we compared the performance of the 2 methods at classifying unknown embryonic statoliths. We found large spatial errors often associated with DFA assignments, even when traditional DFA accuracy assessments indicated the method was performing well. The continuous method provided an improved assessment of uncertainty in assignments. It outperformed the DFA method in classifying unknown embryos to the vicinity of their true source. Geospatial statistics also provided useful information on other range-wide variables, such as adult reproductive abundance. As a proxy for larval supply, such information can aid future assignments of recruits. Our combined analyses help inform sampling designs and motivate the development of a new approach for population connectivity studies.

KEY WORDS: Connectivity · Larval dispersal · *Kelletia kelletii* · Statolith · Geochemical tags · Spatial variation · Geostatistics

INTRODUCTION

Larval dispersal has profound effects on population and community dynamics (Kinlan & Gaines 2003), genetics (Palumbi 1994, Hellberg 2009), and biogeography (Lester & Ruttenberg 2005). Empirical studies (e.g. Jones et al. 1999, 2005, Swearer et al. 1999, Planes et al. 2009) have advanced our understanding of larval dispersal. However, to date, these studies have been limited to cases involving self-

*Corresponding author: skoch@ucla.edu

recruitment (Jones et al. 1999, 2005) or dispersal across a small part of a species' range (Becker et al. 2007, Planes et al. 2009, Carson 2010, Christie et al. 2010, Buston et al. 2012, Almany et al. 2013, Chittaro & Hogan 2013). At present, there are no empirical estimates of demographic connectivity among many populations across a species' entire geographic range (Pineda et al. 2007, but see Walther et al. 2008 for a juvenile dispersal example). Such estimates would allow us to model the spatial and temporal dynamics of meta-populations (Botsford et al. 2009).

Empiricists and modelers have long recognized the need for such global information on species. The goal is to construct a population connectivity matrix (Botsford et al. 2009), in which the key data are the fraction of larvae from each potential source (*j*) traveling to each potential destination (*i*) throughout a species' range (our Fig. 1; Largier 2003, Mitarai et al. 2008).

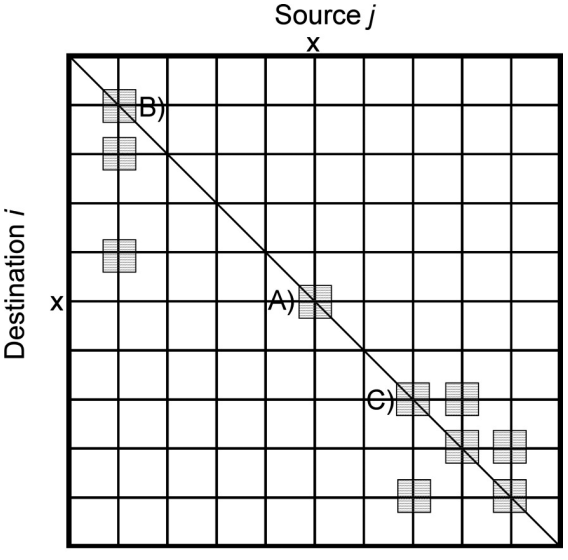

Fig. 1. An idealized population connectivity matrix that describes the relationships among source (*j*) and destination (*i*) patches of propagules. Patches can occur in a variety of configurations, ranging from continuous coastlines to non-continuous reefs, islands, estuaries, marine reserves, etc. Each vertical line indicates a potential source location, and each horizontal line indicates a potential destination location. The diagonal line represents propagules produced at a source location returning to settle at the same location as a destination, sometimes referred to as 'self-recruitment'. Letters indicate the 3 cases of patch configurations characterized by recent larval assignment studies. (A) A case of self-recruitment with propagules at j_x returning to i_x (e.g. Jones et al. 1999, Almany et al. 2007). (B) Propagules are marked at one source location and recaptured at a few destinations (e.g. Jones et al. 2005, Planes et al. 2009). (C) A case of identifying recruits from a small number of sources at a few destinations (e.g. Becker et al. 2007, Carson 2010). Note that none of these cases succeed in fully characterizing the connectivity matrix across a species' range

Some studies have measured components of the matrix in the field. For example, mark-recapture and DNA parentage analysis studies (Jones et al. 1999, 2005, Almany et al. 2007) provide a binary measure of larval dispersal by categorizing settlers as locally produced or not (e.g. A and B in Fig. 1). A few field studies using either DNA parentage analysis (Planes et al. 2009, Buston et al. 2012, Saenz-Agudelo et al. 2012) or natural geochemical tags (Becker et al. 2007, Standish et al. 2008, Carson 2010, Chittaro & Hogan 2013) have been able to estimate exchange of larvae among several locations (C in Fig. 1) along a part of a species' range, an impressive advance toward the construction of a full connectivity matrix. Yet, since these studies did not sample all potential sources, they could not rule out possible contributions from the rest of the species' range. As a result, a risk remains for misidentifying sources and underestimating dispersal distances.

Theoretically, geochemical tagging approaches could characterize the tags of developing larvae from all possible sources, but this potential has not been realized (Campana 1999, Munch & Clarke 2008, Neubauer et al. 2010). Natural geochemical tags, such as otoliths (Campana 1999) and statoliths (Zacherl et al. 2003, Zacherl 2005), are biogenic carbonates, $CaCO_3$ crystals enmeshed within a protein matrix, that begin forming in the embryo at its birth location (Chia et al. 1981). Layers are continually added throughout the embryo's life and become permanently incorporated into the structure. Divalent cations from the surrounding seawater (i.e. Mg^{+2} and Sr^{+2}) co-precipitate with $CaCO_3$. Abiotic factors (e.g. temperature, salinity, chemistry) and biological factors such as growth rate (Carré et al. 2006, Hamer & Jenkins 2007), genetics (Wheeler 1992), and maternal investment (Thorrold & Jones 2006, Lloyd et al. 2008) vary across a species' range and can influence uptake of cations into biogenic carbonates (Kalish 1990, Thorrold & Jones 2006), potentially providing every larva with a geographically-specific geochemical tag. Use of otolith/statolith geochemical tags have so far permitted identification of recruit sources and partial estimates of connectivity (Swearer et al. 1999, Hamer et al. 2005, Becker et al. 2007, Carson 2010).

The potential for geochemical tags to generate a full and robust connectivity matrix has not yet been realized because most natural geochemical tag studies have struggled with common logistical challenges. They may have (1) only sampled a small part of a species' range, (2) under-sampled within sites, (3) sampled at a scale that was too coarse, and/or (4) not characterized temporal variation. It is difficult to

know whether previous studies addressed challenges (2) and (3) above without explicit tests such as a power analysis.

These logistical challenges are compounded by statistical challenges. The analytical framework most frequently applied to geochemical tagging data is discriminant function analysis (DFA). DFA has many shortcomings (White & Ruttenberg 2007), and the most problematic is that it ignores unsampled sources between locations as well as spatial autocorrelation of geochemical tags. Thus, the results of DFA lack spatial continuity and a means to perform spatial uncertainty assessment. DFA is also unable to specify how far away from a sample location assignment predictions hold. Unlike DFA, kriging can estimate continuous spatial patterns from scattered point samples. Kriging is a geospatial statistical method that has been used extensively in geology (Goovaerts 1999) and is increasingly finding application in landscape ecology and genetics (e.g. Manel et al. 2003, Wasser et al. 2004, Murphy et al. 2008). However, the use of kriging in marine ecology has been more limited (Robertson 1987, Legendre & Fortin 1989, Gustafson 1998), and kriging has not been applied to the problem of natural geochemical tagging.

In this study, we analyze natural geochemical tags in embryonic statoliths over the entire range of an open coast marine gastropod, *Kelletia kelletii*. We address each of the common logistical and statistical challenges associated with this approach by characterizing within-site, among-site, and temporal variation in statolith chemistry and by using geospatial statistics (multivariate kriging) to estimate tags at unsampled locations. We test the performance of DFA against that of the new geospatial method developed here by characterizing spatial uncertainty and classifying individuals left out of model development. Last, we show how geospatial statistics can also be used to characterize the strength of potential larval sources using adult abundance and habitat availability, and we demonstrate the utility of this information for evaluating competing assignments to sources with similar elemental signatures.

MATERIALS AND METHODS

Study organism

Kellet's whelk *Kelletia kelletii* (Forbes, 1850) is a neogastropod found on rocky reefs from Monterey, California, USA, to Isla Asunción, Baja California, Mexico (Herrlinger 1981). Adults reproduce once a year, in May to August, at the kelp/sand interface (D. C. Zacherl pers. obs.), where females deposit benthic egg capsules (Rosenthal 1970). Embryos brood within egg capsules, developing statoliths after 15 to 19 d (Zacherl et al. 2003). Veligers hatch after 30 to 34 d (Rosenthal 1970). Laboratory studies suggest a planktonic larval duration of at least 5.5 wk at 15°C (Romero et al. 2012). The part of the statolith formed before hatching can be analyzed using mass spectrometry and used as a tag of a recruit's source location (Zacherl 2005).

Sampling natural tags from sources across the range

SCUBA divers collected mature egg capsules from rocky reefs (15 to 18 m) from mid-June to early August in both 2004 (at 12 sites) and in 2005 (at 17 sites) (Fig. 2, Table 1) to sample natural geochemical tags throughout the entire range of *K. kelletii*. We collected at least 10 broods from each site and froze them at –80°C until analysis.

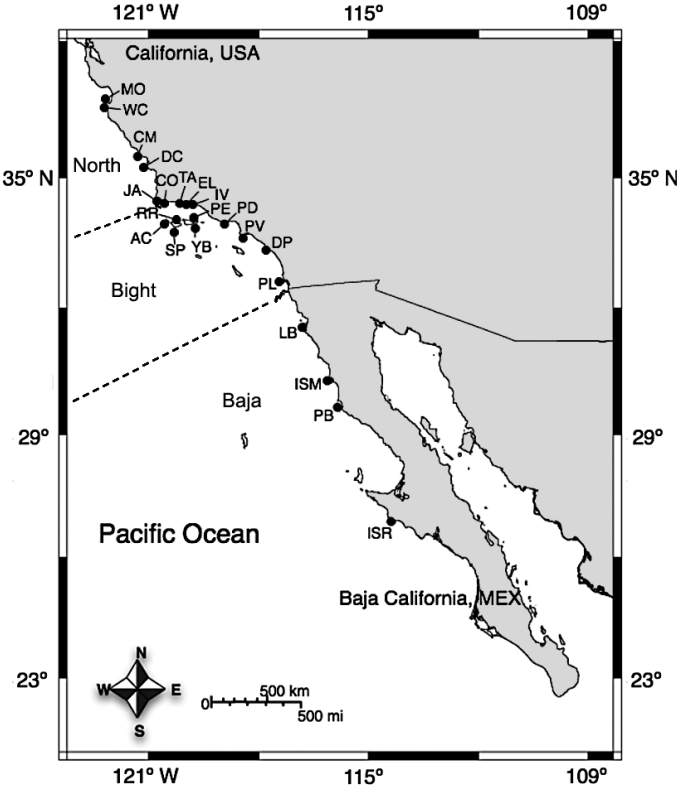

Fig. 2. *Kelletia kelletii*. Egg-mass collection sites for 2004 and 2005. Sites span the entire range of *K. kelletii* to characterize the elemental composition of embryonic statoliths from probable sources of larvae. Site names are coded as in Table 1 and grouped into 3 geographical regions: North, Bight and Baja (see 'Materials and methods')

Table 1. *Kelletia kelletii*. Names, codes and years of egg-mass collection sites, regional classification, GPS locations, number of statoliths sampled per site (N) and average metal/calcium ratios (±1 SE)

Site code	Site name	Latitude (°N)	Longitude (°W)	Year	Statoliths (N)	Mg/Ca (mmol mol^{-1})	Sr/Ca (mmol mol^{-1})	Ba/Ca (µmol mol^{-1})	Ce/Ca (µmol mol^{-1})	Pb/Ca (µmol mol^{-1})
North region										
MO	Monterey	36.6182	121.897	2004	50	1.90 (0.02)	9.31 (0.05)	7.68 (0.12)	0.06 (0.01)	0.19 (0.02)
				2005	50	1.33 (0.02)	9.22 (0.05)	7.09 (0.07)	0.04 (0.002)	1.77 (0.08)
WC	Whalers Cove	36.5207	121.9392	2005	49	1.55 (0.02)	8.89 (0.05)	7.87 (0.09)	0.06 (0.003)	2.13 (0.07)
CM	Cambria	35.5701	121.1252	2005	50	1.83 (0.02)	9.19 (0.06)	11.02 (0.13)	0.08 (0.003)	6.35 (0.41)
DC	Diablo Canyon	35.2245	120.8775	2005	50	1.52 (0.02)	8.90 (0.06)	7.60 (0.11)	0.08 (0.01)	1.33 (0.09)
JA	Jalama	34.4942	120.5045	2004	50	1.91 (0.02)	8.53 (0.04)	7.04 (0.17)	0.16 (0.01)	0.47 (0.17)
Bight region										
CO	Cojo	34.4481	120.4018	2004	50	2.13 (0.04)	9.11 (0.08)	9.11 (0.28)	0.11 (0.01)	0.80 (0.09)
				2005	50	1.73 (0.02)	7.75 (0.07)	6.93 (0.09)	0.15 (0.01)	0.60 (0.05)
AC	Adams Cove	34.0234	120.4357	2005	50	1.83 (0.02)	9.18 (0.06)	6.76 (0.11)	0.05 (0.01)	0.35 (0.04)
RR	Rodes Reef	34.0389	120.1180	2004	49	2.05 (0.03)	9.35 (0.06)	7.74 (0.28)	0.06 (0.01)	0.40 (0.03)
SP	South Point	33.8916	120.1216	2005	48	1.84 (0.03)	9.05 (0.07)	6.69 (0.14)	0.10 (0.01)	0.86 (0.19)
PE	Pelican	34.0274	119.6905	2005	50	1.74 (0.03)	8.52 (0.08)	9.29 (0.23)	0.09 (0.01)	0.46 (0.03)
YB	Yellowbanks	33.9913	119.5646	2004	50	2.06 (0.04)	8.40 (0.05)	5.93 (0.11)	0.05 (0.004)	0.38 (0.05)
				2005	50	1.64 (0.02)	8.69 (0.06)	7.39 (0.10)	0.04 (0.003)	0.77 (0.03)
TA	Tajiguas	34.4592	120.0949	2004	50	1.95 (0.03)	8.17 (0.07)	6.33 (0.08)	0.06 (0.003)	0.34 (0.01)
EW	Ellwood	34.4271	119.9239	2004	50	2.15 (0.03)	8.07 (0.10)	6.03 (0.20)	0.08 (0.01)	0.74 (0.50)
IV	Isla Vista	34.4047	119.8675	2004	50	2.19 (0.04)	8.57 (0.06)	8.11 (0.14)	0.10 (0.004)	0.66 (0.02)
				2005	49	1.84 (0.03)	9.16 (0.07)	9.76 (0.23)	0.17 (0.01)	0.96 (0.05)
PD	Point Dume	33.9935	118.8048	2004	50	1.80 (0.02)	7.44 (0.08)	5.55 (0.10)	0.13 (0.01)	0.48 (0.10)
				2005	50	2.00 (0.04)	8.69 (0.07)	9.65 (0.52)	0.14 (0.01)	0.54 (0.08)
PV	Palos Verdes	33.7105	118.3177	2004	50	1.92 (0.04)	8.29 (0.06)	8.79 (0.39)	0.08 (0.01)	0.41 (0.03)
				2005	50	2.28 (0.04)	8.73 (0.06)	8.47 (0.14)	0.10 (0.004)	0.71 (0.02)
DP	Dana Point	33.4757	117.7333	2004	50	2.17 (0.04)	7.73 (0.08)	7.00 (0.21)	0.15 (0.01)	0.48 (0.04)
				2005	50	1.83 (0.02)	8.15 (0.05)	7.55 (0.10)	0.09 (0.01)	2.07 (0.24)
PL	Point Loma	32.6933	117.2709	2004	50	2.04 (0.02)	9.05 (0.08)	12.94 (0.39)	0.05 (0.003)	1.52 (0.16)
Baja region										
LB	La Bufadora	31.7233	116.7175	2005	50	1.60 (0.02)	8.85 (0.06)	6.52 (0.09)	0.10 (0.01)	0.57 (0.04)
ISM	Isla San Martin	30.4853	116.0975	2005	50	1.64 (0.02)	8.45 (0.06)	6.32 (0.08)	0.01 (0.002)	3.02 (0.10)
PB	Punta Baja	29.9216	115.7714	2005	49	1.53 (0.02)	8.99 (0.07)	6.61 (0.07)	0.12 (0.02)	2.85 (0.29)
ISR	Isla San Roque	27.1545	114.3602	2005	50	1.90 (0.02)	9.66 (0.06)	7.66 (0.14)	0.03 (0.004)	1.27 (0.09)

Ensuring sufficient sampling within sites

We used Monte Carlo simulations of a DFA to determine a statolith sampling strategy that would capture variation in elemental signatures within each site. We used data from Zacherl (2005) to parameterize the variance in metal/calcium (Me/Ca) ratios among statoliths within broods, among broods within sites, and among sites ('training data'). These data consisted of 7 Me/Ca ratios (Zn/Ca, Sr/Ca, Ba/Ca, Ce/Ca, Pb/Ca, Mg/Ca, and Mn/Ca) recorded for 1384 individual embryonic statoliths in 140 broods distributed among 7 sites (2 to 7 broods per site, 7 to 10 statoliths per brood). Training data were $\log_{10}(x+1)$ transformed for normality, standardized, and then transformed using a principal components rotation to remove correlations among elemental ratios ('transformed training data').

We carried out Monte Carlo simulations using pseudo-random numbers drawn from normal distributions describing among-site, among-brood, and within-brood variance, estimated by maximum likelihood in a hierarchical linear model fit to the transformed training data. Simulated sample designs assumed 37 sites and varied the number of broods per site from 5 to 95 and the number of statoliths per brood from 1 to 10. For each sample design, we performed a minimum of 1000 Monte Carlo realizations. Random samples of 2 to 100 simulated statoliths were then drawn from the simulated pool of all statoliths from a site (i.e. without respect to brood). We rotated the resulting simulated sample data back into the original coordinate space (to account for cross-correlation among elemental ratios) and subjected the back-transformed simulated data to DFA. Classification success to the site level was assessed using the

discriminant function derived from the full, simulated data set (model success) and by cross-validation with 10% of data withheld (cross-validation success).

The mean and standard error of model and cross-validation success were then plotted vs. the number of individual statoliths sampled from the site pool under different sampling designs (statoliths/brood and broods/site). We chose the sample sizes and brood pooling strategy to give the maximum mean model and cross-validation classification success with the lowest standard error of classification within the constraints of sampling effort. The number of statoliths per site had more effect on classification success than the number of broods per site. Regardless of the number of broods sampled per site, classification success plateaued after 30 statoliths. The outcome of these simulations resulted in our chosen sampling strategy: to pool 500 larvae from 10 broods per site and subsample 50 statoliths per site. These analyses were carried out in MATLAB R12 using the Statistics Toolbox (Mathworks).

Statolith elemental analysis

We isolated embryonic statoliths of *K. kelletii* and analyzed them for trace elements (Mg, Sr, Ba, Pb, and Ce) using techniques detailed in Zacherl (2005), Koch (2008) and the Supplement at www.int-res.com/articles/suppl/m508p033_supp.pdf. All isolation steps were completed in an analytical chemistry laboratory at the Marine Science Institute, University of California Santa Barbara (UCSB). Fifty larvae from 1 egg capsule were haphazardly selected from each of 10 broods per site (500 larvae total) for cleaning. Of these, 50 statoliths per slide were haphazardly selected for analysis using laser ablation inductively coupled plasma mass spectrometry (LA-ICP-MS). We conducted all elemental analyses using a UP-213 laser ablation system (Solid state Nd:YAG, UP-213; New Wave Research) coupled to an ICP-MS (Finnegan Element 2). We standardized elemental counts using a Me/Ca ratio.

Classical assignment approach using ANOVA, MANOVA, and DFA

We compared samples using nested multivariate analysis of variance (MANOVA) with 2 fixed factors (region, site [region]) to determine among-site and among-region spatial variability of trace elements in embryonic statoliths within each year (2004 and 2005). All data were $\log_{10}(x + 1)$ transformed to ensure they met the assumptions of analysis of variance (ANOVA) and MANOVA, including normality and homogeneity of variances (Huberty & Olejnik 2006).

We grouped sites into 3 distinct geographic regions *a priori* (north of Point Conception [North], Southern California Bight [Bight] and Baja California [Baja]) based on topography and oceanographic conditions (Zacherl et al. 2003, Zacherl 2005) (Table 1). The colder California Current bathes sites north of Point Conception. The warmer, saltier California Counter Current influences the sites south of Point Conception.

We used *a posteriori* contrast tests to indicate which regions and which sites within regions were significantly different from each other. Then, we ran a DFA using all Me/Ca ratios. We used a jack-knife serial-deletion cross-validation technique to estimate the success rate of DFA at assigning statoliths to site nested within region.

We compared 2 years (2004 and 2005) of data from a subset of sites (Monterey, Jalama, Ellwood, Yellowbanks, Point Dume, and Dana Point) using a nested ANOVA (year, site [year]) and MANOVA (year, site [year]) to determine the temporal variability of trace elements in statoliths. Then, we used jack-knife serial-deletion cross-validation to estimate the success rate of DFA at assigning statoliths to year at each site. The DFA was run assuming equal-probability prior distributions.

To estimate a p-value for the jack-knife reclassification success of the DFAs, we analyzed the dataset using a randomization bootstrapping technique (White & Ruttenberg 2007). In total, 5000 iterations of the model were run to estimate the probability of our result being significantly different from random by chance alone. We ran all statistical analyses using the program JMP version 8.0 (SAS Institute) and MATLAB R13 (Mathworks).

Geospatial statistics

Kriging can interpolate continuous spatial patterns from scattered point samples (Isaaks & Srvivastava 1989, Cressie 1993, Goovaerts 1997, Chiles & Delfiner 2012) by predicting values at unsampled locations based on spatial autocorrelation between pairs of sampled points (variogram model). Each unsampled point can be predicted as a weighted average of all sampled points, where the weights are derived from the variogram function. Kriging reproduces the data values at actual sample points. When data are normally distributed or can be transformed,

and their mean and variance are stationary over the study area, kriging yields the best, unbiased linear predictor at unsampled locations and provides an estimate of uncertainty (Chiles & Delfiner 2012).

We used multivariate ordinary kriging (Chiles & Delfiner 2012) to estimate the joint spatial pattern of all 5 Me/Ca ratios (see the Supplement). Me/Ca ratios were $\log_{10}(x + 1)$ transformed for normality, centered, standardized, and transformed into principal components using the pooled covariance matrix before kriging. We performed leave-one-site-out cross-validation to assess accuracy of kriging predictions and report cross-validation root-mean-square errors as a measure of prediction error at unsampled locations (Fig. S2 in the Supplement; Deutsch & Journel 1998).

Continuous assignment and spatial uncertainty assessment using geospatial statistics

Positional uncertainty in assignment can be derived by applying the same assignment principle used to determine classification success in DFA, while considering the kriging-predicted elemental values at unsampled locations between sample sites. In DFA classification, an individual of unknown origin is assigned to the group (site) to which it is closest in multivariate space. Multivariate distance is measured by the Mahalanobis distance metric, which measures the distance between a point and the centroid of a group in multivariate space assuming a multivariate normal distribution. If the multivariate normal assumption holds, this leads to a maximum likelihood classification (Huberty & Olejnik 2006). To derive an equivalent continuous assignment method based on kriged geochemical signatures and associated measures of positional error, we first define a multivariate normal (MVN) distribution of the elemental signatures z_m at each m of the M possible locations on the coast:

$$z_m \sim \mathrm{MVN}(\mu_m, C_{mij}) \quad (1)$$

where μ_m is the kriging mean at location m. C_{mij} is the $M \times K \times K$ matrix consisting of the M variance-covariance matrices for locations along the coast. Each location-specific variance-covariance matrix C_{ij} is $K \times K$, where K is the number of elements, and is defined as follows:

$$C_{ij} = \begin{bmatrix} s_{11} + \sigma_1 & s_{12} & s_{13} & \dots & s_{1j} \\ . & . & & & \\ . & & . & & \\ . & & & . & \\ s_{i1} & s_{i2} & s_{i3} & \dots & s_{ij} + \sigma_k \end{bmatrix} \quad (2)$$

where s_{ij} is the within-site covariance of the Me/Ca ratios of elements i and j, and σ_k is the kriging variance of element k. At sample locations, the mean and covariance will be equal to the sample mean and variance because the kriging variance is 0 (Deutsch & Journel 1998). At unsampled locations, the predicted mean is the kriging mean, and the predicted variance for each elemental ratio (diagonal of the covariance matrix) reflects the sum of sampling error (s_{ij}) and spatial uncertainty (σ_k). Then, for each of the N individuals sampled in a year, the Mahalanobis distance to each of the M possible coastal locations is calculated. The location with the minimum absolute value of the Mahalanobis distance is the position along the coast to which that individual is assigned.

To measure positional error in assignment, we carried out assignment in this way and then calculated the along-coast distance between the maximum likelihood assignment and the true location of origin of each individual embryonic statolith, and we summarized positional error using the mean and quantiles of this 'distance error' distribution.

Comparison of DFA and continuous geospatial methods

To compare the classification success resulting from DFA to that from the continuous geospatial method, we applied each method to re-classify embryonic statoliths from known sites. Frequency histograms of along-coast re-classification assignments for statoliths from each site of origin were used to compare results across methods. For simplicity of visualization, figures show results mapped vs. latitude rather than along-coast distance, but all analyses of distances between sites for comparing DFA and continuous geospatial methods refer to distances measured along the coastline (including shortest distance across water to islands for island sites). Note that, in some cases, sites are much further apart in terms of along-coast distance than they appear when mapped vs. latitude.

To compare the overall performance of DFA vs. the continuous geospatial method when confronted with statoliths from a source (i.e. a source not used in model fitting), we conducted leave-one-site-out cross-validation exercises at a subset of 3 sites. In each exercise, all information pertaining to one site was completely removed, and all stages of DFA and geospatial analyses were repeated (including variogram model inference and kriging). Then, the 50 statoliths from the left-out site were classified using the cross-

validation discriminant function and kriging atlas. Frequency histograms of along-coast assignments for statoliths from each left-out site were used to compare performance across methods.

Source strength

We also show how geospatial statistics can be used to assess the relative magnitude of potential larval sources across the range, which may provide prior probability information useful in distinguishing sources difficult to separate by natural geochemical tags alone. We gathered reproductive-adult density data from 61 sites (26 of our own, 35 from CRANE; see the Supplement). We used kriging to estimate adult abundances at all potential sources across the entire range as a proxy of source strength by combining adult density with spawning habitat data collected from satellites and aerial photographs (see Broitman & Kinlan 2006). Adult density data were $\log_{10}(x + 1)$ transformed before kriging to normalize data. We calculated the omni-directional sample variogram, using the Euclidean distance between (latitude, longitude) points. Use of latitude, longitude allowed us to include both island and coastline sites in the same analysis. We fit an exponential variogram model to the sample variogram using a weighted non-linear least-squares algorithm (Pardo-Igúzquiza 1999; see the Supplement). Because the sample variogram exhibited continuity near the origin, we elected to fit a model without a nugget effect. We used the ordinary kriging package in GSLIB (Deutsch & Journel 1998) to predict adult density at the midpoints of grid cells defined by 1 km intervals along the 1:250 000 World Vector Shoreline (Soluri & Woodson 1990) (starting at a point 36.7821°N, 121.7990°W and proceeding southward along the coast in 1 km intervals). For islands, 1 km intervals were defined based on the northernmost point on the island coastline, proceeding counterclockwise.

RESULTS

Spatial variation of natural geochemical tags in 2004 and 2005

Embryonic statolith Me/Ca ratios collected in 2004 differed significantly among all 12 sites (MANOVA, followed by Bonferroni-corrected contrasts, $p < 0.0001$; Table S2 in the Supplement) and 2 regions (MANOVA, $p < 0.0001$; Table S2). Compared with statoliths from the Bight, embryonic statoliths from the North had higher Sr/Ca and Ce/Ca ratios but lower Mg/Ca, Ba/Ca, and Pb/Ca ratios (see Table 1 for per-site averages used to calculate regional averages).

Using DFA, we generated canonical variance plots for sites and regions using embryonic statoliths from 2004 (Fig. 3A,C). The group centroids for each site occupied unique locations in canonical space, but 95% confidence ellipses of the centroids typically overlapped with at least 1 other site (Fig. 3A); the regional group centroids and confidence ellipses occupied different regions in canonical space (Fig. 3C). The magnitude of the vectors of the standardized discriminant functions indicated that Ba/Ca and Sr/Ca ratios played the most important roles in discriminating statoliths among sites (Fig. 3A), versus Pb/Ca and Sr/Ca ratios for among-region discrimination (Fig. 3C). The directions of the vectors depict the regional trends (Fig. 3C) in Me/Ca ratio.

Leave-one-out jack-knife validation — used to determine whether the chemical composition of a statolith collected in 2004 could predict its site and region of formation — successfully assigned statoliths to their site of origin 56% of the time compared to 8% by chance alone (Fig. 3A, Table S3 in the Supplement). Statoliths from Monterey and Point Loma were distinct from statoliths from almost all other sites and had the highest classification success (82% and 88% respectively). Grouping sites into the 2 geographic regions sampled in 2004 (North and Bight) increased the classification success to 78% compared to 50% by random chance alone (Fig. 3C, Table S3).

The chemical composition of embryonic statoliths collected in 2005 also differed significantly among all 17 sites (MANOVA, followed by Bonferroni-corrected contrasts, $p < 0.0001$; Table S2) and all 3 regions (MANOVA, followed by Bonferroni-corrected contrasts, $p < 0.0001$; Table S2). Embryonic statoliths from the North had the highest Sr/Ca, Ba/Ca and Pb/Ca ratios (Table 1). The Bight had the highest Mg/Ca and Ce/Ca ratios (Table 1).

The DFA canonical variance plots for sites and regions using embryonic statoliths from 2005 (Fig. 3B,D) show group centroids for each site occupying unique locations in canonical space, but as with 2004, 95% confidence ellipses of the centroids typically overlapped with at least 1 other site (Fig. 3B); the regional group centroids and confidence ellipses occupied very different locations in canonical space (Fig. 3D). The magnitude of the vectors of the standardized discriminant functions indicated that Ba/Ca and Pb/Ca played the most important roles in discriminating statoliths among sites (Fig. 3B), versus Ba/Ca and

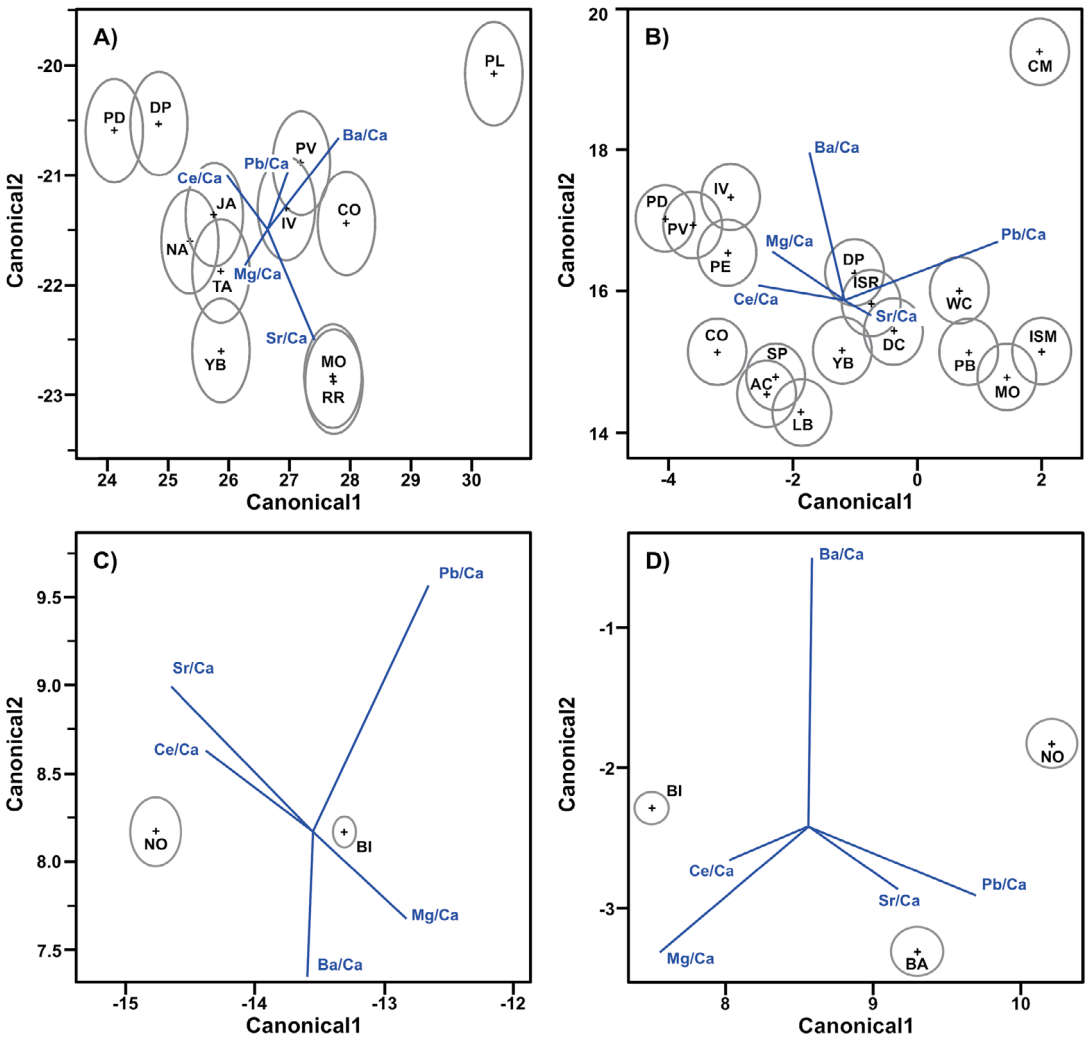

Fig. 3. *Kelletia kelletii*. Plots depicting scores for the first 2 canonical axes of discriminant function analysis that tested for spatial variation in the elemental composition of embryonic statoliths collected at sites in (A) 2004 and (B) 2005 and sites nested within regions in (C) 2004 and (D) 2005. Ellipses are the 95% confidence intervals of the group means. The length and direction of bi-plot rays reflect the relative contribution of each element to discriminating among regions. Letters in (A,B) correspond to site codes in Table 1. Regions: NO, North; BI, Bight; BA, Baja

Mg/Ca for among-region discrimination (Fig. 3D). The directions of the vectors (Fig. 3D) were again consistent with the regional trends in Me/Ca ratio.

The leave-one-out jack-knife validation success for 2005 was 70% (*t*-test, p = 0.0002) successful at assigning all statoliths to their site of origin compared to 6% expected by chance alone (Table S3). Some sites were distinct from almost all other sites and had very high classification success. For example, Isla San Martin had classification success of 100%, and Cambria (96%) (Table S3), Cojo (88%), Monterey (88%), and Palos Verdes (82%) also had relatively high classification success rates (Table S3). Grouping sites into 3 geographic regions (North, Bight, and Baja) increased the classification success to 81% (*t*-test, p = 0.0002) compared to 33.3% by random chance alone (Fig. 3D, Table S3).

Temporal variation in natural geochemical tags

The multi-elemental chemistry of statoliths among sites and regions varied significantly between 2004 and 2005 (MANOVA, p < 0.0001; Table S4 in the Supplement), as did individual Me/Ca ratios in statoliths at the majority of sites examined (Table S5 in the Supplement). Mg/Ca ratios varied significantly between years at every site examined (Table S5). The Ce/Ca ratio was the most temporally stable, varying significantly between years at 4 of the 7 sites

(Table S5). Mg/Ca, Sr/Ca and Ce/Ca ratios varied in a consistent way between regions from year to year (Fig. 4). Sr/Ca and Ba/Ca ratios were higher in the North than the Bight in both years, whereas Mg/Ca and Ce/Ca ratios were significantly higher in the Bight than the North in both years. Ba/Ca and Pb/Ca ratios did not show consistent spatial trends between years (Fig. 4). For instance, the Pb/Ca ratio was highest in the Bight in 2004 but was much higher in the North during 2005 (Fig. 4).

Geostatistical approach

Variogram models fit to empirical variogram estimates (Fig. S1 in the Supplement) yielded estimates of the range parameter, a measure of the 'patch scale,' or characteristic length scale of autocorrelation. The weighted average range parameter for elemental signatures was 102 km in 2004 and 183 km in 2005, with 100 km for the first principal component (PC1) and 140 km for PC2 in 2004 and with 324 km for PC1 and 73 km for PC2 in 2005 (Table S6 in the Supplement). Principal component axis loadings and elemental signature correlation matrices are shown in the Supplement (Tables S7 & S8).

The along-coast predictions of Me/Ca ratios show a mixture of meso-scale variability (10s to 100s km) and more localized small-scale variability (10s km). The large-scale regional patterns were less prominent. Three Me/Ca ratios (Sr/Ca, Mg/Ca, and Ba/Ca) tended to be more smoothly distributed. This resulted in lower uncertainties than for the more spatially uncertain patterns of Ce/Ca and Pb/Ca ratios (Fig. 4). The area between 33.5 and 34.5° N latitude shows the highest spatial variability for all the elements except Pb/Ca and, to a lesser extent, Mg/Ca (Fig. 4).

Since no sites were sampled south of 32.5° N in 2004, kriging predictions for all elements for the southern part of the study area in 2004 are equal to the mean Me/Ca ratio for all sites within the 900 km kriging search radius, and uncertainty is equal to the total among-site variance. Note that discontinuities in the kriging predictions occur at the southern edge of the domain in 2004 because the far northern sites fall out of the 900 km search window.

Spatial uncertainty assessment

We estimated the spatial uncertainty of assignments using the continuous geospatial method and compared it to DFA by building frequency histograms of maximum likelihood re-classification assignment locations for embryonic statoliths (Fig. 5). Use of the continuous method (right-hand panel of each pair of plots in Fig. 5) corrects for the 'no other source' assumption in DFA by giving the best estimate of correct assignment based on kriging inferences about populations between sampled locations. In the cases of Cojo and Monterey embryonic statoliths in 2005 (Fig. 5B,C), the DFA method yielded 88% reclassification success for both sites (Table 2, Table S3). In contrast, a continuous assignment method reveals that the distance error associated with an 88% assignment success could range from 37 km (Cojo 2005) to 315 km (Monterey 2005). Eighty percent of statoliths could be assigned to Monterey within a 10 km range in 2005, but one would have to consider sources >200 km away to get the 88% reclassification success reported by DFA. Cojo 2005 had smaller distance error, but only 31% of statoliths could be assigned within 10 km. In years (2004; Fig. 5A) and regions (Baja, Fig. 5D) with less sampling effort, both methods had greater error in assignment (greater spread in histograms in Fig. 5A,D), but the continuous geospatial method allowed that uncertainty to be spread over any site along the coast, whereas for DFA, the mis-classifications were necessarily (and misleadingly) clustered at the discrete set of sites included in the analysis.

Leave-one-site-out cross-validation comparison

A more powerful test of the real-world performance of assignments using the DFA vs. continuous geospatial methods is provided by the leave-one-site-out cross-validation analysis (Fig. 6). In this test, the DFA method was constrained to assign unknown statoliths to one of the limited set of known sites (which did not include the true source), whereas the continuous method considered all potential sources. In all cases tested, assignments using the continuous geospatial method outperformed or matched the DFA. The continuous method assigned unknown statoliths to the vicinity of their site of origin more often than other locations, with a high degree of fidelity (Fig. 6A,B right-hand panels). For example, the continuous method assigned 62% of statoliths from Monterey (2005) and 66% from Cambria (2005) to within 100 km along-coast of their site of origin, even though the site of origin was not included in the kriging atlas (Fig. 6A,B right-hand panels). Along-coast distances of these assignments ranged from 23 to 93 km (0.15° to 0.62° latitude; along-coast distances

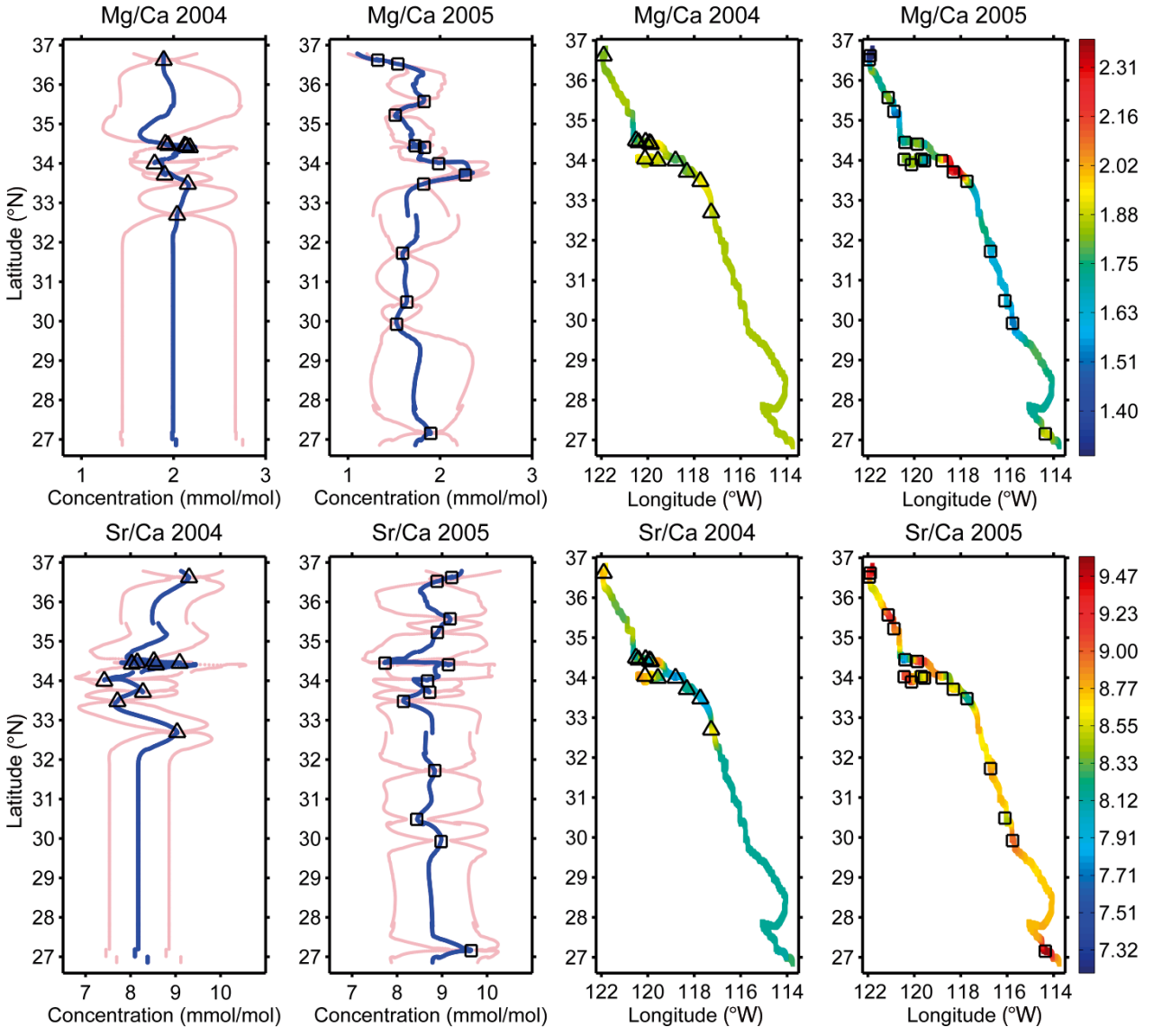

Fig. 4. Range-wide natural geochemical tag atlas. Observed natural geochemical tags (Mg/Ca, Sr/Ca, Ba/Ca, Ce/Ca, and Pb/Ca) in *Kelletia kelletii* embryonic statoliths in 2004 (triangles, 1st column) and 2005 (squares, 2nd column) are shown with the continuous kriged interpolation (blue lines) and 95% confidence limits (pink lines). For visualization of spatial patterns along the coastline, the results are plotted in latitude-longitude space in the 3rd (2004) and 4th (2005) columns using a colormap that varies from blue (minimum) to red (maximum)

and latitudes can be correlated using Fig. 2). In the case of Palos Verdes (2004), where both methods performed equally poorly overall, the continuous method had the advantage of more accurately representing the uncertainty of assignments (Fig. 6C). The DFA method gave very high assignment frequencies to incorrect sites, giving the false impression of accuracy. In 2004, DFA assigned 98% of statoliths from Palos Verdes to sites more than 100 km along-coast from the true origin (Fig. 6C, left-hand panel). These mis-assignments included 7 sites to the north (MO, JA, TA, CO, IV, RR, and PD) and 1 site to the south (PL) with along-coast distances of 138 to 832 km (0.28° to 2.91° latitude) (Figs. 2 & 6C). In 2005, DFA assigned 72% from Palos Verdes to sites more than 100 km along-coast from the true origin (Fig. 6D, left-hand panel). These mis-assignments included 4 sites to the north (CO, IV, AC, and PD) and 1 site to the south (ISR) with along-coast distances of 138 to 1205 km (0.28° to 6.56° latitude) (Figs. 2 & 6D). Note that while unknown statoliths are often classified nearest the site of origin by the continuous method,

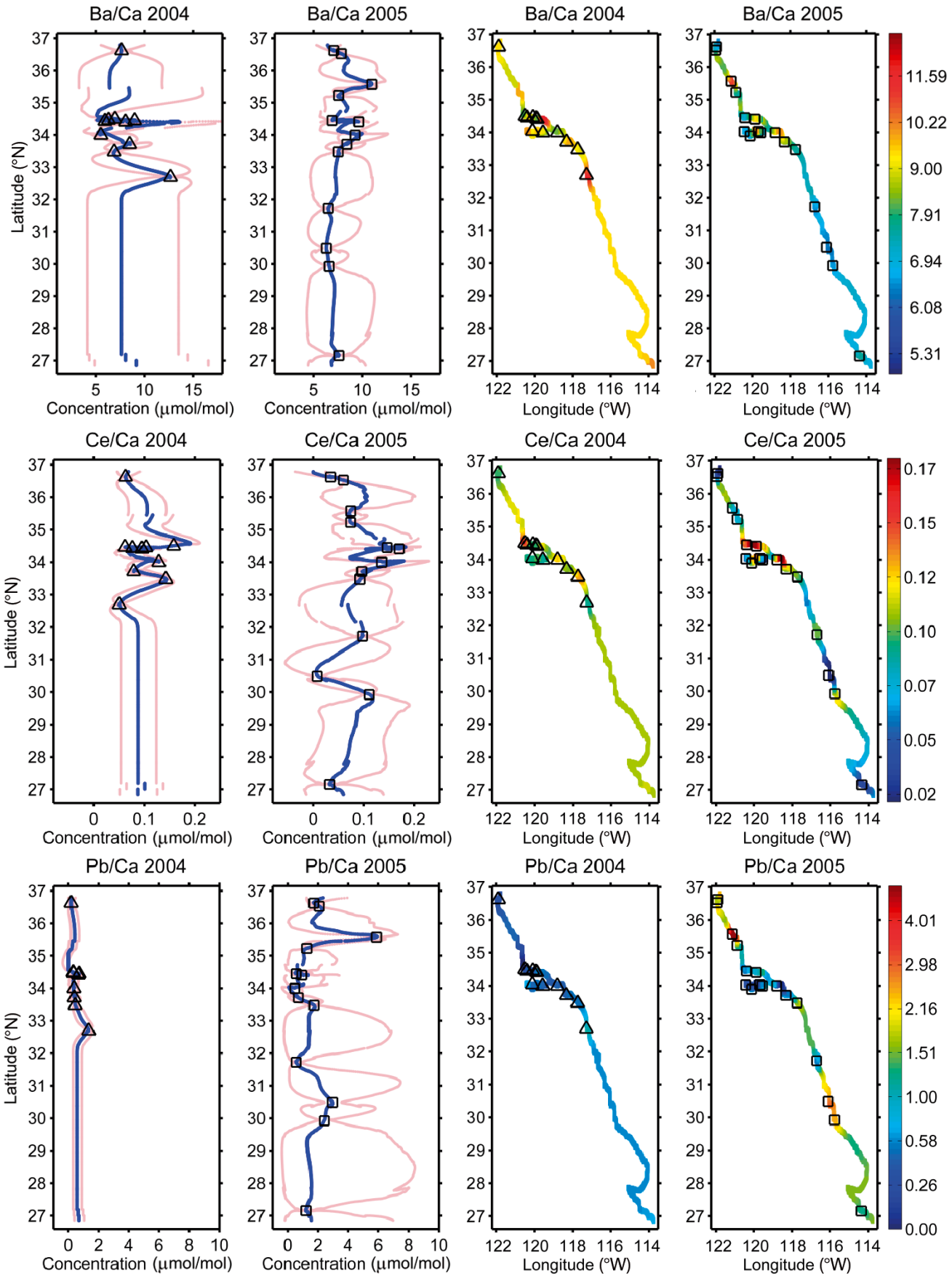

Fig. 4 (continued)

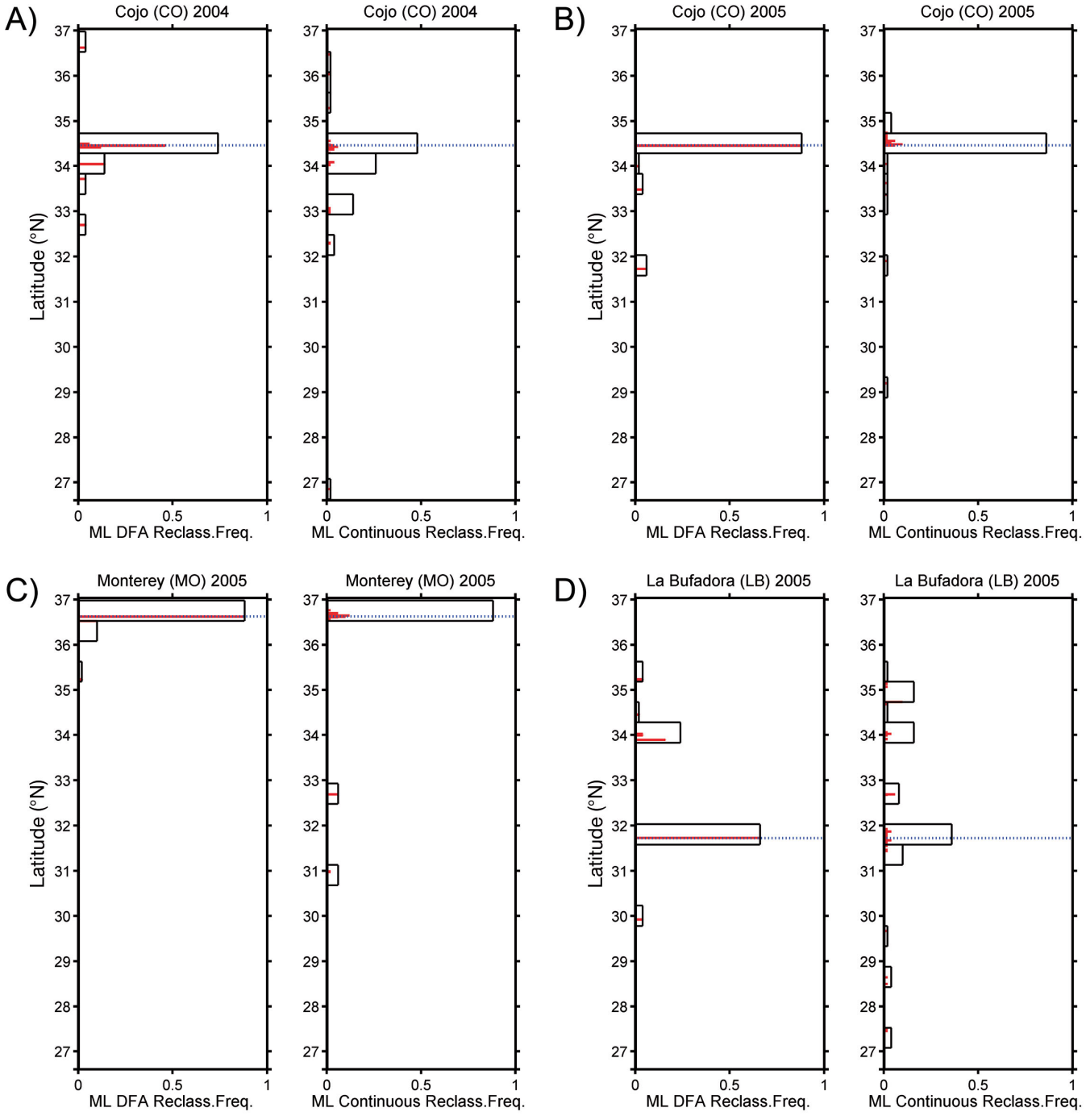

Fig. 5. Comparison of discriminant function analysis (DFA) and continuous re-classification of individuals from known sources. Each pair of plots compares the frequency histogram of the maximum likelihood (ML) re-classification assignment locations for individuals originating at a given site (true site of origin, indicated by the blue dotted reference line) for the DFA method (left-hand panel of each pair of plots) vs. continuous method (right-hand panel of each pair of plots). DFA assignments can only occur to one of the sampled locations. The continuous method provides a means to consider all potential sources and thereby evaluate the spatial uncertainty associated with DFA assignments. The true site of origin was included in the training sets for both methods. Solid red bars are histograms at finest possible resolution given the kriging atlas (~1 km along-coast bins), plotted vs. latitude. Outlined black bars are the result of summing the fine-scale histogram along the latitude axis in 0.45° (~50 km) bins. Note that histograms were calculated as a function of latitude for visualization only. Frequencies calculated in along-coast distance bins (not shown) differ from frequencies calculated in the latitudinal bins shown here. To represent the range of results, 4 examples are shown based on re-classification of embryonic statoliths originating at sites (A) Cojo in 2004, (B) Cojo in 2005, (C) Monterey in 2005, and (D) La Bufadora in 2005

Table 2. Re-classification success and distance error at given distance thresholds for embryonic statolith sources in (A) 2004 and (B) 2005, comparing discriminant function analysis (DFA) with the continuous assignment method. DFA distance error was calculated using the continuous approach and represents the distance away from the source over which one would need to bin the continuous results to get the percentage re-classification success reported by DFA. Thus, it is a measure of the spatial uncertainty of DFA assignments. Also shown is the distribution of percentages of re-classification success obtained using the continuous method by binning at various distances from sources. See Table 1 for site codes

Site code	DFA reclass. success (%)	DFA dist. error (km)	Reclassification success continuous method (%) 1 km	5 km	10 km	20 km	50 km	100 km	200 km	500 km	1000 km
(A) 2004											
MO	82.0	194.1	2.5	8.5	14.3	37.9	64.7	65.8	83.3	100.0	100.0
JA	66.0	114.8	0.0	31.8	44.0	50.4	53.9	61.4	79.7	100.0	100.0
TA	50.0	82.4	3.9	23.0	23.4	23.7	24.4	62.1	76.6	100.0	100.0
CO	46.0	60.7	0.0	5.8	19.1	22.4	39.3	72.7	76.9	97.6	99.9
EW	52.0	60.5	10.8	26.4	30.0	31.6	36.0	69.6	79.6	95.8	100.0
IV	58.0	251.5	5.7	11.5	13.4	13.8	18.1	42.0	47.3	83.7	91.1
RR	36.7	22.4	0.0	0.0	0.0	30.8	73.4	87.4	89.4	100.0	100.0
PD	64.0	79.5	0.0	5.3	10.6	29.6	63.5	64.4	94.7	100.0	100.0
YB	54.0	34.8	6.0	13.7	23.5	48.7	56.1	71.5	72.6	95.8	100.0
PV	48.0	125.3	0.0	0.0	0.0	0.0	19.4	26.2	65.1	85.5	100.0
DP	28.0	43.1	0.0	0.0	1.0	12.3	32.1	36.6	77.3	93.6	100.0
PL	88.0	276.4	0.0	13.7	19.3	52.1	73.0	73.7	74.2	100.0	100.0
Mean	56	112.1	2.4	11.6	16.6	29.4	46.2	61.1	76.4	96.0	99.2
(B) 2005											
MO	88.0	315.2	0.0	36.5	79.7	87.0	87.3	87.5	87.7	90.9	100.0
WC	71.4	389.0	3.9	22.2	36.0	38.2	39.1	43.6	68.9	73.1	100.0
CM	96.0	991.8	0.0	28.0	43.2	80.3	93.2	93.4	93.7	94.0	96.4
DC	54.0	344.3	1.9	7.5	10.9	21.5	31.9	35.2	49.4	85.8	100.0
CO	88.0	37.1	1.6	6.0	31.0	55.8	89.5	90.2	92.1	97.4	100.0
IV	65.3	32.2	0.0	0.5	7.5	27.5	77.2	86.4	95.1	97.4	100.0
PE	66.0	119.7	3.5	9.2	17.8	23.5	35.6	40.5	83.9	90.0	100.0
AC	74.0	331.9	7.6	30.7	41.4	42.4	46.3	55.2	70.1	79.9	100.0
PD	54.0	108.1	0.0	1.7	8.0	11.9	24.2	49.4	87.6	90.1	100.0
YB	68.0	263.8	1.6	9.3	18.7	19.7	21.4	22.6	36.1	97.6	100.0
SP	25.0	49.0	0.0	0.0	0.0	10.7	25.1	44.3	49.0	57.6	100.0
PV	82.0	37.4	0.0	4.5	14.2	49.8	83.5	84.3	92.0	94.2	100.0
DP	48.0	292.6	0.0	0.1	2.8	15.6	23.7	24.7	41.7	79.4	100.0
LB	66.0	409.7	2.0	5.7	15.3	39.4	45.5	46.3	54.2	87.6	100.0
ISM	100.0	387.5	0.0	1.1	2.6	17.3	86.6	87.6	87.9	100.0	100.0
PB	59.2	143.1	0.0	0.0	0.0	2.5	51.6	55.1	74.5	94.2	100.0
ISR	78.0	734.3	0.0	6.0	10.7	41.6	75.0	75.4	75.7	76.3	93.9
Mean	70	293.3	1.3	9.9	20.0	34.4	55.1	60.1	72.9	87.4	99.4

in some cases, substantial mis-assignment rates may occur to distant sites, as occurred in the Palos Verdes analysis in 2004 and 2005 (Fig. 6C,D). More information than provided by elemental signatures alone (e.g. source strength, see below) would be required to reduce these rates of mis-classification. However, in cases where uncertainty in the kriging atlas was high (e.g. Fig. 6C), the continuous method accurately represented greater uncertainty in assignment from the uncertainty in unsampled sites' elemental signatures. The continuous method also revealed effects of variation in the along-coast resolution of the atlas, reflected in the spread of fine-scale assignments around sites of origin (e.g. compare red bars in Fig. 6A,D right-hand axes).

Accounting for source strength: incorporating continuous along-coast predictions of reproductive adult abundance

The scale of spatial autocorrelation in adult *Kelletia kelletii* abundance was 201 km (Fig. S3 in the Supplement). Estimated reproductive adult abundances of *K. kelletii* were highest in the middle (~34° to 31° N) and lowest at the northern and southern parts of the geographic range (Fig. 7). The 2 highest observed peaks in adult abundance occurred near major upwelling centers just south of Point Conception (California, USA) and near Punta Colonet (Baja California, Mexico) (Fig. 7, Table S1 in the Supplement). They shared a similar scale of spatial autocorrelation as

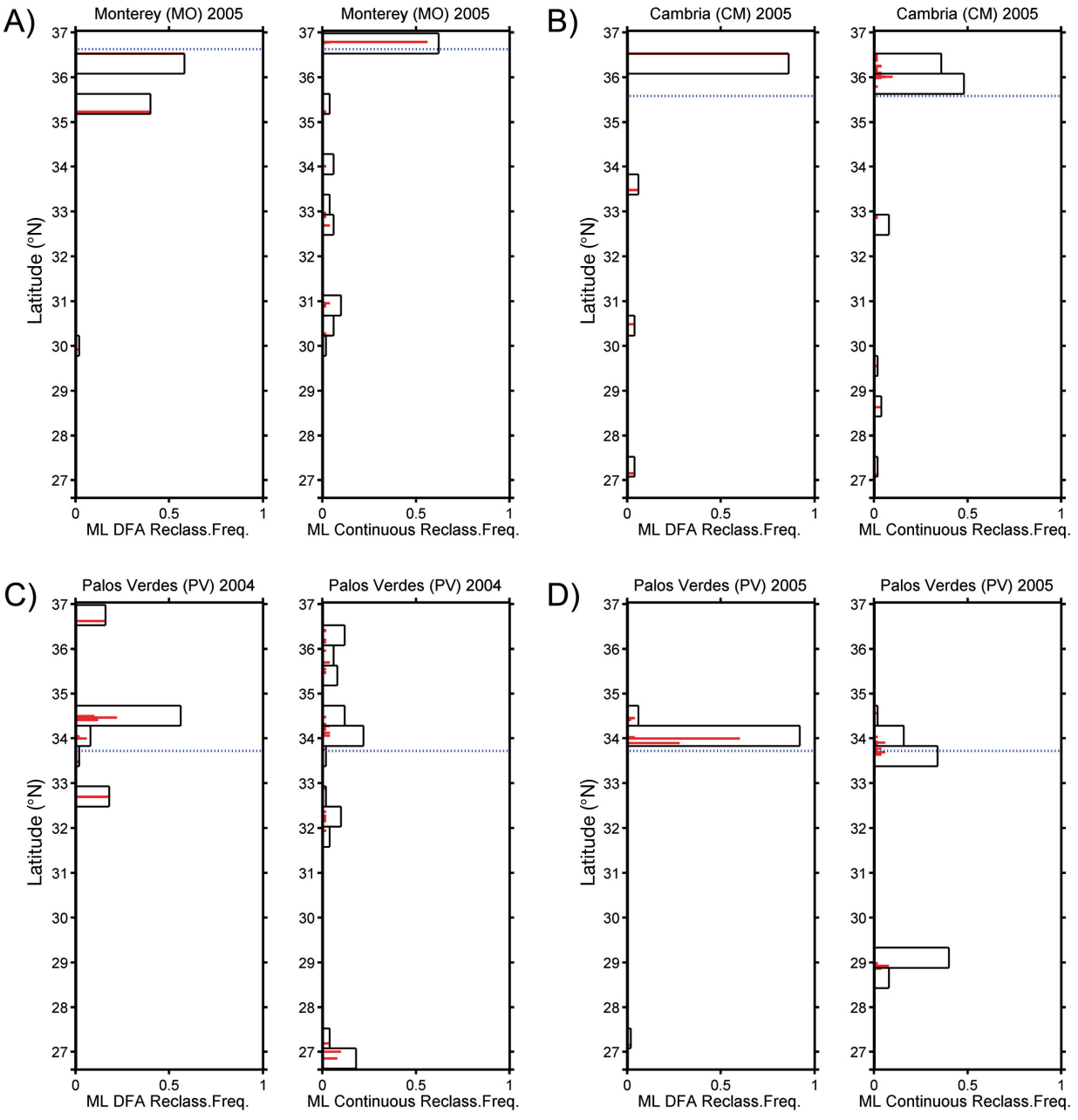

Fig. 6. Leave-one-site-out cross-validation. For 4 sets of 50 statoliths, the site of origin was completely left out of all stages of discriminant function analysis (DFA) and continuous analyses, and then those statoliths were classified by each technique. Results are compared in each pair of plots A–D. Symbology is as in Fig. 5. The excluded sites were (A) Monterey 2005, (B) Cambria 2005, (C) Palos Verdes 2004, and (D) Palos Verdes 2005. Note that histograms were calculated as a function of latitude for visualization only. Frequencies calculated in along-coast distance bins (not shown) differ from frequencies calculated in the latitudinal bins shown here. Percentages of unknown statoliths classified to within 100 km along-coast of their true origin for the 2 methods were as follows: (A) DFA: 58%, Continuous: 62%; (B) DFA: 0%, Continuous: 66%; (C) DFA: 2%, Continuous: 2%; (D) DFA: 28%, Continuous: 48%

previously reported for kelp surface canopy cover (188 km) (Broitman & Kinlan 2006). We found the lowest densities of adults at several sites along the Big Sur Coast (Cambria, San Simeon, La Cruz) in central California and on Santa Rosa Island (Johnsons Lee, Beacon Reef) in the Santa Barbara Channel (Fig. 7, Table S1). Low habitat availability accounted for lower abundances elsewhere, including much of the southernmost part of the range.

The potential value of using the abundance of reproductive adults as a proxy for larval source strength can be seen by re-visiting the Palos Verdes leave-

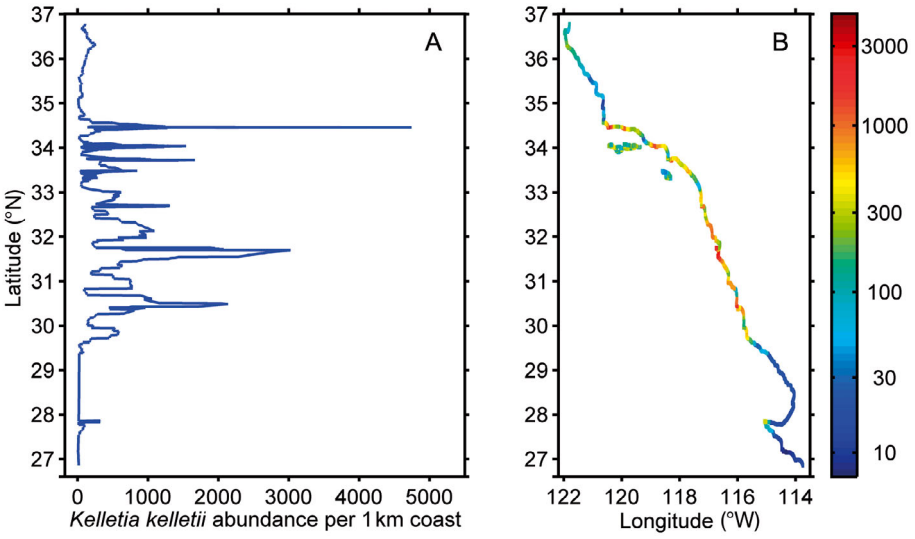

Fig. 7. *Kelletia kelletii*. Range-wide pattern of reproductive adult abundances (number of individuals per km of coastline), estimated by kriging density estimates from transect surveys conducted in 2004 and 2005 and multiplying by habitat area per unit coastline from kelp canopy-cover remote sensing. Results are plotted (A) vs. latitude or (B) in latitude-longitude space using a colormap that varies from blue (minimum) to red (maximum)

one-site-out cross-validation analysis (Fig. 6C,D). In both years, statoliths from Palos Verdes were misclassified at fairly high rates to sites in 2 distinct clusters in the Baja region, 100s of km south of Palos Verdes. Examining the pattern of adult abundance (Fig. 7) reveals that both of those peaks fall in areas with virtually no possible source of *K. kelletii* larvae, which if incorporated into the analysis as a prior probability could improve assignment rates using this kriging atlas. In 2005, when the geochemical sampling was more extensive, the addition of adult abundance as a source-strength proxy would allow almost all unknown statoliths to be definitively assigned to the vicinity of the correct site (i.e. by combining the pattern shown in the right-hand axes of Fig. 6D with Fig. 7).

DISCUSSION

Our sampling design and statistical approach allowed us to confront many of the challenges that thwart geochemical tagging studies. We sampled across the species' entire range, as opposed to sampling only a small subset of potential sources. We used Monte Carlo simulations to calculate the number of statoliths we needed to sample within sites in order to ensure accurate representation of within-site variability of geochemical tags. We tested for among-site and among-time variation using classical discriminant analyses. Then, we critically examined the performance of DFA in this application against an alternative continuous geospatial method. With any estimate of dispersal or connectivity based on point samples (e.g. the classical DFA approach), there is always a chance that assignments to sources are wrong (Campana 1999, Munch & Clarke 2008). Without explicitly testing for positional error, there is no way to know the robustness of resultant predictions. If researchers only sample across a portion of the species' geographic range, then the problem is compounded with unknown error of potential misassignment or underestimation of dispersal distance. Even if samples are taken throughout a species' range, it remains logistically challenging to sample every possible source. The continuous geospatial method took advantage of natural spatial autocorrelation and used kriging to interpolate tags at unsampled locations. This allowed us to estimate a larval source atlas from all potential sources and to estimate the spatial error of assignments associated with DFA. Comparison of DFA to the continuous geospatial method revealed a serious problem with the application of linear discriminant approaches to assignments in open coast systems. Because DFA does not include the majority of potential sources along a coastline, it can make false high-accuracy assignments to sites that are not the true source. DFA does not provide an estimate of spatial uncertainty that would allow detection of such errors.

Using standard DFA, sites were significantly different, with respectively 56% and 70% reclassification successes for 2004 and 2005, compared to 8% and 6% by chance alone. The classic approach would be to group sites into regions to further increase classification success (i.e. 78% in 2004, 81% in 2005; Table S3). However, doing this sacrifices the ability to build a detailed connectivity matrix to estimate larval dispersal at fine spatial scales (Neubauer et al. 2010, Miller et al. 2013). Furthermore, DFA provides no

estimate of spatial uncertainty associated with later assignments of recruits to potential sources. Most importantly, DFA ignores potential unsampled sources along the coastline when making assignments.

The geospatial method allowed us to assign unknown individuals to a continuous coastline with measures of spatial uncertainty. We found that spatial uncertainty was large, averaging 112 km for 2004 and 293 km for 2005 (Table 2). A comparison of the 2 methods (left versus right-hand panels of each pair of plots in Fig. 5) reveals that classical DFA is constrained to assign an unknown recruit to only those precise locations sampled, despite the fact that nearby potential sources may have a similar chemical signature. Thus, DFA 'appears' to assign unknown individuals more accurately. But this is only because it ignores the spatial error of assignment success since sites between locations are not considered. A continuous assignment method can account for potential unsampled sources and give an estimate of spatial uncertainty to each assignment.

This point is underscored by the leave-one-site-out cross-validation comparison of DFA and continuous geospatial methods when confronted with individuals from unknown sources (Fig. 6). DFA makes very high (apparent) accuracy assignments to the wrong sources (Fig. 6A–D). The geospatial method can make similarly high accuracy assignments to the vicinity of the correct source when justified by a full consideration of all possible sources along the coast (Fig. 6A,B) but also accurately represents the alongcoast uncertainty when the natural geochemical tag atlas is uncertain (Fig. 6C,D).

In many cases where uncertainty in the underlying kriging atlas makes assignment purely based on elemental signatures difficult (Fig. 6C,D), continuous geospatial statistics can provide additional insight and improve assignment based on range-wide proxies for larval source strength (Fig. 7). Our exercise combining source strength with a continuous assignment method is similar to emerging approaches that combine multiple independent data sets to estimate sources and/or connectivity (Gaggiotti et al. 2002, 2004, Smith & Campana 2010, Rushing et al. 2014). For example, to assign wintering songbirds to breeding grounds, Rundel et al. (2013) combined 2 independent data sets — genetic and stable isotope — in a Bayesian framework. While not specifically aiming to estimate connectivity, Rundel et al. (2013) demonstrated that the integration of the 2 data sets resulted in assignment estimates with higher spatial precision than could be achieved using one method alone.

For a continuously distributed species when only a subset of sites is sampled, the accuracy of DFA will be a function of the selection of sites sampled, rather than the true accuracy of assignments. By sampling at a scale larger than the underlying scale of geochemical autocorrelation, one can improve the accuracy of apparent DFA re-classification success. However, this is a trivial — and misleading — result of the fact that the DFA accuracy calculation ignores all populations between sample locations. A researcher would not know the error in their sampling design and re-assignment accuracy without testing for spatial autocorrelation. Sampling sites at a spatial scale that is too coarse would decrease the ability to detect spatial autocorrelation. Thus, in the context of open-coast populations, DFA will tend to report the highest rates of classification success in the situations when it is doing worst. In the extreme case where a few, widely separated sites are chosen, DFA is likely to report very high re-classification accuracy. The continuous assignment method considers all possible sources and reveals that such DFA assignments have high spatial uncertainty and contain little information. Using a continuous assignment method does not guarantee improved spatial certainty, as shown by our re-classification experiments for poorly sampled years/regions (Fig. 5A,D). However, it does guarantee that spatial uncertainty will be accurately represented in the presence of unknown sources, subject to the assumptions of the geospatial modeling technique used. Such measures of spatial uncertainty can be used to (1) assign weight to the evidence for particular assignments, (2) guide future sampling, (3) determine the scale to which a given source atlas can measure dispersal, and (4) determine the spacing of sites at which recruits should be collected.

Our analyses of the 2004 data revealed that extending statolith sampling south of Point Loma, USA, down to Punta Eugenia, Mexico, would improve our assignments. This conclusion was driven by the high kriging uncertainties in the Baja region in 2004 (Fig. 4) and examination of the low percentage of holdout data that were within ±1 SD of the prediction bounds for elements in 2004 (Table S9 in the Supplement). When we performed leave-one-out cross-validation of elemental kriging data, only a small percentage of the left-out data fell within ±1 SD of predicted values (e.g. 25% for Ce/Ca in 2004, Table S9, compared to an expectation of ~68% given the normally distributed error assumption). This inaccuracy in the kriging model guided our choice of sampling sites in 2005, which improved our spatial characterization of tags in that year (Fig. 4; Table S9,

column 2). As this demonstrates, geospatial methods can readily be used to optimize sampling and produce a source atlas that maximizes the information available on which to base assignments for a given number of samples (see Brus & Heuvelink 2007).

We were also able to determine the spatial scale to which our source atlas was capable of resolving dispersal patterns. The median resolution of our 2004 source atlas (i.e. along-coast distance at which 50% of re-classifications were correct; Table 2) was ~63 km. In 2005, the improved spatial sampling regime increased our median source atlas resolution to 43 km. However, these are range-wide averages. A detailed model of spatial variation in natural tags can identify areas where larval dispersal can and cannot be finely resolved. Re-classification, leave-one-out cross-validation, and related simulation studies can be used to assess the performance of an atlas for each sampled and unsampled location along the coast, and further sampling can be used to tune the atlas. This approach represents a powerful new tool for the design and optimization of natural tag atlases.

The spatial scale of autocorrelation in natural geochemical tags is also useful for planning the next stage in a tagging study. Knowledge of the spatial pattern of tag variability can be used to determine the optimal location and spacing of recruit collection sites. This would maximize the power to make inferences regarding sources. Given the more robust extent of sampling undertaken in 2005, our spatial scale of autocorrelation of elements was 183 km. This means that a sampling design with sufficient sites spaced within this scale coast-wide could represent the spatial variation in geochemical tags across the range. However, in areas of high spatial variability — such as 4 where 2 water masses collide — sampling would need to be conducted at a smaller scale. This is obvious from examination of the kriging of elements shown in Fig. 4 (e.g. note the exceptional variation in Sr/Ca across the Channel Islands). A similar pattern of small-scale spatial variability has been observed in trace elements along the open-coast of northern California, an area of strong upwelling (Miller et al. 2013).

More formal methods of geospatial optimization (e.g. Brus & Heuvelink 2007) could be used to plan and test different recruit sampling designs. Other interpolation techniques, such as universal kriging (which allows incorporation of environmental covariates) or spatial models estimated in a hierarchical Bayesian framework, could also be applied (Munch & Clarke 2008, Carroll et al. 2010) and may improve estimation of the continuous geochemical atlas, reducing uncertainty. Regardless, it would seem prudent to abandon a DFA approach in geochemical tagging studies for open-coast marine species in favor of continuous methods, such as the geospatial method presented here.

Acknowledgements. Funding from the National Science Foundation (OCE 0351860 to D.C.Z., Steven D. Gaines and R.R.W.), the Partnership for Interdisciplinary Studies of Coastal Oceans (PISCO), and the Canon National Parks Science Scholars Program (C.W.) supported this work. B.P.K. was supported during the writing phase by NOAA Contract No. DG133C07NC0616 with Consolidated Safety Services. Thank you to the staff (Michael Sheehy and Kate Shears) at the University of California Santa Barbara (UCSB) Analytic Lab. A flotilla of SCUBA divers and boat tenders helped to collect samples, including Alison Haupt, Elizabeth Hoaglund-Joubert, Julie Hopper, Julio Lorda, Rodrigo Beas-Luna, Juleen Dickson, Brian Cheng, Michael Navarro, Diana Lloyd, and Derek Smith. Thanks also to the boat captains, Capt. Shane Anderson of the fleet of *Fish* boats at UCSB and Capt. Ray and Capt. Mark of the *Garibaldi* at the California Department of Fish and Game. Thank you to the Department of Biological Science at the California State University Fullerton for their generous support and use of facilities. Thanks also to Will White and an anonymous reviewer for their helpful comments that much improved the manuscript.

LITERATURE CITED

Almany GR, Berumen ML, Thorrold SR, Planes S, Jones GP (2007) Local replenishment of coral reef fish populations in a marine reserve. Science 316:742–744

Almany G, Hamilton R, Bode M, Matawai M and others (2013) Dispersal of grouper larvae drives local resource sharing in a coral reef fishery. Curr Biol 23:626–630

Becker BJ, Levin LA, Fodrie FJ, McMillan PA (2007) Complex larval connectivity patterns among marine invertebrate populations. Proc Natl Acad Sci USA 104: 3267–3272

Botsford LW, White JW, Coffroth MA, Paris CB and others (2009) Connectivity and resilience of coral reef metapopulations in marine protected areas: matching empirical efforts to predictive needs. Coral Reefs 28:327–337

Broitman B, Kinlan B (2006) Spatial scales of benthic and pelagic producer biomass in a coastal upwelling ecosystem. Mar Ecol Prog Ser 327:15–25

Brus D, Heuvelink G (2007) Optimization of sample patterns for universal kriging of environmental variables. Geoderma 138:86–95

Buston PM, Jones GP, Planes S, Thorrold SR (2012) Probability of successful larval dispersal declines fivefold over 1 km in a coral reef fish. Proc R Soc Lond B Biol Sci 279: 1883–1888

Campana S (1999) Chemistry and composition of fish otoliths: pathways, mechanisms and applications. Mar Ecol Prog Ser 188:263–297

Carré M, Bentaleb I, Bruguier O, Ordinola E, Barrett N, Fontugne M (2006) Calcification rate influence on trace element concentrations in aragonitic bivalve shells: evi-

dences and mechanisms. Geochim Cosmochim Acta 70: 4906–4920
Carroll C, Johnson D, Dunk J, Zielinski W (2010) Hierarchical Bayesian spatial models for multispecies conservation planning and monitoring. Conserv Biol 24:1538–1548
Carson H (2010) Population connectivity of the Olympia oyster in Southern California. Limnol Oceanogr 55:134–148
Chia FS, Koss R, Bickell LR (1981) Fine structural study of the statocysts in the veliger larva of the nudibranch, *Rostanga pulchra.* Cell Tissue Res 214:67–80
Chiles J, Delfiner P (2012) Geostatistics: modelling spatial uncertainty, 2nd edn. John Wiley & Sons, Hoboken, NJ
Chittaro P, Hogan J (2013) Patterns of connectivity among populations of a coral reef fish. Coral Reefs 32:341–354
Christie MR, Johnson DW, Stallings CD, Hixon MA (2010) Self-recruitment and sweepstakes reproduction amid extensive gene flow in a coral-reef fish. Mol Ecol 19: 1042–1057
Cressie N (1993) Statistics for spatial data. John Wiley & Sons, New York, NY
Deutsch C, Journel A (1998) GSLIB geostatistical software library and user's guide. Oxford University Press, New York, NY
Forbes E (1850) On the species of Mollusca collected during the surveying voyages of the Herald and Pandora, by Capt. Kellett, R.N., C.B. and Lieut. Wood, R.N. Proc Zool Soc Lond 18:270–274
Gaggiotti OE, Jones F, Lee WM, Amos W, Harwood J, Nichols RA (2002) Patterns of colonization in a metapopulation of grey seals. Nature 416:424–427
Gaggiotti OE, Brooks SP, Amos W, Harwood J (2004) Combining demographic, environmental and genetic data to test hypotheses about colonization events in metapopulations. Mol Ecol 13:811–825
Goovaerts P (1997) Geostatistics for natural resources evaluation. Oxford University Press, New York, NY
Goovaerts P (1999) Geostatistics in soil science: state-of-the-art and perspectives. Geoderma 89:1–45
Gustafson E (1998) Quantifying landscape spatial pattern: What is the state of the art? Ecosystems 1:143–156
Hamer P, Jenkins G (2007) Comparison of spatial variation in otolith chemistry of two fish species and relationships with water chemistry and otolith growth. J Fish Biol 71: 1035–1055
Hamer P, Jenkins G, Gillanders B (2005) Chemical tags in otoliths indicate the importance of local and distant settlement areas to populations of a temperate sparid, *Pagrus auratus.* Can J Fish Aquat Sci 62:623–630
Hellberg M (2009) Gene flow and isolation among populations of marine animals. Annu Rev Ecol Evol Syst 40: 291–310
Herrlinger T (1981) Range extension of *Kelletia kelletii.* Veliger 24:78
Huberty CJ, Olejnik S (2006) Applied MANOVA and discriminant analysis, 2nd edn. John Wiley & Sons, Hoboken, NJ
Isaaks E, Srvivastava R (1989) An introduction to applied geostatistics. Oxford University Press, New York, NY
Jones G, Milicich M, Emslie M, Lunow C (1999) Self-recruitment in a coral reef fish population. Nature 402:802–805
Jones GP, Planes S, Thorrold SR (2005) Coral reef fish larvae settle close to home. Curr Biol 15:1314–1318
Kalish J (1990) Use of otolith microchemistry to distinguish the progeny of sympatric anadromous and non-anadromous salmonids. Fish Bull 88:657–666
Kinlan B, Gaines S (2003) Propagule dispersal in marine and terrestrial environments: a community perspective. Ecology 84:2007–2020
Koch S (2008) Exploring the use of statoliths of *Kelletia kelletii* as natural tags to estimate population connectivity across a species' range. MS thesis, California State University, Fullerton, CA
Largier J (2003) Consideration in estimating larval dispersal distances. Ecol Appl 13:71–89
Legendre P, Fortin MJ (1989) Spatial pattern and ecological analysis. Vegetatio 80:107–138
Lester SE, Ruttenberg BI (2005) The relationship between pelagic larval duration and range size in tropical reef fishes: a synthetic analysis. Proc R Soc Lond B Biol Sci 272:585–591
Lloyd DC, Zacherl DC, Walker S, Paradis G, Sheehy M, Warner RR (2008) Egg source, temperature and culture seawater affect elemental signatures in *Kelletia kelletii* larval statoliths. Mar Ecol Prog Ser 353:115–130
Manel S, Schwartz M, Luikart G, Taberlet P (2003) Landscape genetics: combining landscape ecology and population genetics. Trends Ecol Evol 18:189–197
Miller SH, Morgan SG, White JW, Green PG (2013) Interannual variability in an atlas of trace element signatures for determining population connectivity. Mar Ecol Prog Ser 474:179–190
Mitarai S, Siegel D, Winters K (2008) A numerical study of stochastic larval settlement in the California Current system. J Mar Syst 69:295–309
Munch S, Clarke L (2008) A Bayesian approach to identifying mixtures from otolith chemistry data. Can J Fish Aquat Sci 65:2742–2751
Murphy M, Evans J, Cushman S, Storfer A (2008) Representing genetic variation as continuous surfaces: an approach for identifying spatial dependency in landscape genetic studies. Ecography (Cop) 31:685–697
Neubauer P, Shima JS, Swearer SE (2010) Scale-dependent variability in *Forsterygion lapillum* hatchling otolith chemistry: implications and solutions for studies of population connectivity. Mar Ecol Prog Ser 415:263–274
Palumbi S (1994) Genetic divergence, reproductive isolation, and marine speciation. Annu Rev Ecol Syst 25: 547–572
Pardo-Igúzquiza E (1999) VARFIT: a fortran-77 program for fitting variogram models by weighted least squares. Comput Geosci 25:251–261
Pineda J, Hare J, Sponaugle S (2007) Larval transport and dispersal in the coastal ocean and consequences for population connectivity. Oceanography 20:22–39
Planes S, Jones G, Thorrold S (2009) Larval dispersal connects fish populations in a network of marine protected areas. Proc Natl Acad Sci USA 106:5693–5697
Robertson G (1987) Geostatistics in ecology: interpolating with known variance. Ecology 68:744–748
Romero M, Walker K, Cortex C, Sanchez Y and others (2012) Larval diel vertical migration of the marine gastropod *Kelletia kelletii* (Forbes, 1850). J Mar Biol 2012: 386575
Rosenthal R (1970) Observations on the reproductive biology of the Kellet's whelk, *Kelletia kelletii.* Veliger 12: 319–324
Rundel CW, Wunder MB, Alvarado AH, Ruegg KC and others (2013) Novel statistical methods for integrating genetic and stable isotope data to infer individual-level migratory connectivity. Mol Ecol 22:4163–4176

Rushing CS, Ryder TB, Saracco JF, Marra PP (2014) Assessing migratory connectivity for a long-distance migratory bird using multiple intrinsic markers. Ecol Appl 24: 445–456

Saenz-Agudelo P, Jones G, Thorrold S, Planes S (2012) Patterns and persistence of larval retention and connectivity in a marine fish metapopulation. Mol Ecol 21: 4695–4705

Smith S, Campana S (2010) Integrated stock mixture analysis for continous and categorical data, with application to genetic–otolith combinations. Can J Fish Aquat Sci 67: 1533–1548

Soluri E, Woodson V (1990) World vector shoreline. Int Hydrogr Rev 67:27–35

Standish JD, Sheehy M, Warner RR (2008) Use of otolith natal elemental signatures as natural tags to evaluate connectivity among open-coast fish populations. Mar Ecol Prog Ser 356:259–268

Swearer S, Caselle J, Lea D, Warner R (1999) Larval retention and recruitment in an island population of a coral-reef fish. Nature 402:799–803

Thorrold S, Jones G (2006) Transgenerational marking of embryonic otoliths in marine fishes using barium stable isotopes. Can J Fish Aquat Sci 63:1193–1197

Walther B, Thorrold S, Olney J (2008) Geochemical signatures in otoliths record natal origins of American shad. Trans Am Fish Soc 137:57–69

Wasser S, Shedlock A, Comstock K, Ostrander E, Mutayoba B, Stephens M (2004) Assigning African elephant DNA to geographic region of origin: applications to the ivory trade. Proc Natl Acad Sci USA 101:14847–14852

Wheeler A (1992) Mechanisms of molluscan shell formation. In: Bonucci E (ed) Calcification in biological systems. CRC Press, Boca Raton, FL, p 179–216

White JW, Ruttenberg BI (2007) Discriminant function analysis in marine ecology: some oversights and their solutions. Mar Ecol Prog Ser 329:301–305

Zacherl D (2005) Spatial and temporal variation in statolith and protoconch trace elements as natural tags to track larval dispersal. Mar Ecol Prog Ser 290:145–163

Zacherl D, Paradis G, Lea D (2003) Barium and strontium uptake into larval protoconchs and statoliths of the marine neogastropod *Kelletia kelletii.* Geochim Cosmochim Acta 67:4091–4099

Editorial responsibility: Steven Morgan, Bodega Bay, California, USA

Submitted: October 18, 2013; Accepted: May 17, 2014
Proofs received from author(s): July 24, 2014